UNICA UNIVERSITÀ DEGLI STUDI DI CAGLIARI

IRIS Università di Cagliari

UNICA IRIS Institutional Research Information System

**This is the Author's submitted manuscript version of the following contribution:**

Nastaran Arab, Lida Fotouhi, Maryam Shokouhi, Masoud A. Mehrgardi, and Andrea Salis. A multichannel closed bipolar platform to visual electrochemiluminescence sensing of caffeic acid: Potential for multiplex detection. Analytica Chimica Acta, 1287 (2024) 342087. **DOI:**

**The publisher's version is available at:**

**https://doi.org/10.1016/j.aca.2023.342087**

**When citing, please refer to the published version.**

This full text was downloaded from UNICA IRIS https://iris.unica.it/

# A multichannel closed bipolar platform to visual electrochemiluminescence sensing of caffeic acid: Potential for multiplex detection

*Nastaran Arab [a], Lida Fotouhi [a,b*], Maryam Shokouhi [c], Masoud A. Mehrgardi[c] and Andrea Salis [d,e]*

[a] *Department of Analytical Chemistry, Faculty of Chemistry, Alzahra University, Tehran, Iran*

[b] *Analytical and Bioanalytical Research Centre (ABRC), Alzahra University, Tehran, Iran*

[c] *Department of Chemistry, University of Isfahan, Isfahan 81746-73441, Iran*

[d] *Department of Chemical and Geological Sciences, University of Cagliari, CSGI & CNBS, Cittadella Universitaria, SS 554 Bivio Sestu, 09042 Monserrato (CA), Italy*

[e]*Consorzio Interuniversitario Sistemi a Grande Interfase (CSGI), Florence, Italy*

*Corresponding author: E-mail addresses: lfotouhi@alzahra.ac.ir; Tel.: +98 21 88044040; Fax: +98 21 88035187*

## Abstract

In this study, a fully-featured electrochemiluminescence (ECL) sensing platform based on a multichannel closed bipolar system (closed-BP, C-BP) for the determination of caffeic acid (CA) was successfully developed. The system comprises three individual reservoirs connected to each other by two pairs of gold rods as bipolar electrodes. Moreover, a single pair of gold rods functions as the driving electrodes. Due to configuration consisting of three channels and double-bipolar electrodes, the detection of CA was accomplished in two oxidation and reduction pathways within a single device. Firstly, through close observation of the reactions occurring within the device and utilizing a universal pH indicator and bipolar electrodes, a precise mechanism for the current bipolar systems was initially proposed. Then, the concentration of CA was monitored in the reporting chamber through the following ECL intensities resulting from luminol oxidation and $H_2O_2$. The monitoring process was performed using both a photomultiplier tube (PMT) and a digital camera. In the process of analyte oxidation, the PMT and visual (camera)-based detection exhibited a linear response from 5 μmol $L^{-1}$ to 700 μmol $L^{-1}$ (limit of detection (LOD) 1.2 μmol $L^{-1}$) and 50 μmol $L^{-1}$ to 600 μmol $L^{-1}$ (LOD 14.8 μmol $L^{-1}$), respectively. In the analyte reduction pathway, the respective values were 30 μmol $L^{-1}$ to 450 μmol $L^{-1}$ (LOD 8.6 μmol $L^{-1}$) and 55 μmol $L^{-1}$ to 400 μmol $L^{-1}$ (LOD 21.2 μmol $L^{-1}$), for the PMT and visual-based detection, respectively. Our experiments have demonstrated the practical application of the sensor array for efficient and high-performance analysis. This innovative design holds significant potential for diverse fields and paves the way for the development of a user-friendly device.

*Keywords:* 3D printed microchannels; Closed bipolar electrode; Electrochemiluminescence imaging; Gold rod; Caffeic Acid

## 1. Introduction

In recent years, the bipolar electrochemistry (BPE) and bipolar electrochemiluminescence (BP-ECL) sensing platform have garnered remarkable attention in the biosensor and sensor field due to its essential advantages, such as its low cost, simplicity, portability, and ability to perform multiplex analysis. The absence of a direct connection between external potential instruments and sensing electrodes makes this platform highly appealing [1, 2]. A bipolar configuration involves an electrical conductor placed within either a single solution (open-BP, O-BP) or two distinct solutions (closed-BP, C-BP). This conductor is positioned between two driving electrodes that are connected to an external power supply [3, 4]. By applying a sufficiently high voltage to the driving electrodes, an interfacial potential difference is generated between the bipolar electrodes and the solution they come into contact with. As a consequence, cathodic and anodic overpotentials occur on opposing sides of the bipolar electrodes, thereby triggering faradaic reactions taking place on the bipolar electrodes [5].

The BPE charge balance specifies the detection performance of this setup because there is a direct connection between two reactions occurring on both sides of bipolar electrodes [6-8]. In the C-BP system, the two poles of the bipolar electrodes are positioned in distinct compartments, each containing different fluids, so the current flows exclusively through the bipolar electrodes. The reaction occurring within the sensing reservoir is manifested in the reporting reservoir. Hence, by capturing signals from one pole, the reaction taking place on the other pole of the bipolar electrodes can be detected. The current efficiency of the C-BP-ECL system theoretically reaches nearly 100%. [9].

The transduction of a faradaic current into a visual readout has been accomplished by employing various reporting methods, including fluorescence [10], electrochromic [11], light-emitting diode [12], as well as metal films electrodissolution [13]. Among the various available detection methods, ECL-based systems are extensively acknowledged for their exceptional sensitivity. ECL is the emission of light in close proximity to an electrode, which occurs as a consequence of an electrochemical reaction. In this process, a luminophore undergoes excitation to an excited state through an exergonic redox reaction and transitions back to the ground state by emitting a photon [14]. The ECL assay has garnered significant interest owing to its numerous advantages, including rapid response, high sensitivity, and selectivity, minimal background signal, compatibility with solution-phase analysis, and enhanced control over the position and timing of light emission [15, 16]. These

characteristics make ECL highly suitable for readout in BPE systems [2, 17]. The utilization of C-BP-ECL greatly enhances the remarkable advancements of BPE sensing applications, enabling their implementation in a wider range of analytical scenarios compared to conventional wired electrodes [18]. Until now, numerous C-BP-ECL systems have been developed for the detection of proteins [19-23], nucleic acids [24, 25] cells [2, 26] and enzymes [27-29].

For example, in 2019, Bagherie et al. presented a highly sensitive strategy for the ultrasensitive immunosensing of prostate-specific antigens based on a visual-readout C-BP-ECL system. They utilized two stainless steel sheets and a small segment of an archival compact disk with a gold reflective layer as the driving and bipolar electrodes, respectively. Their approach relied on integrating the hydrogen evolution reaction at the cathodic pole and the ECL of luminol-loaded within the MIL-53(Fe)-$NH_2$ in the anodic pole. After conducting the procedure for modifying gold anodic bipolar electrode, they monitored the ECL signal using both a PMT and a digital camera [19].

In 2022, a “color switch” ECL biosensor was constructed by Chen et al. for detecting the miRNA-141. It consisted of two reservoirs and a constant resistor, and both ends were connected to the driving anode and the bipolar cathode. Taking inspiration from the principle that parallel resistance reduces the overall resistance and increases the total current in a circuit, they introduced a constant resistance in parallel with the bipolar cathode to decrease the total resistance of the circuit. This modification was caused to enhance the ECL signal and improve the detection sensitivity of miRNA-141 under a specific driving voltage [25].

In 2018, Ge et al. fabricated a disposable paper-based analytical device comprised of a closed bipolar electrode for the ECL detection of intracellular $H_2O_2$ and the number of cancer cells. They employed wax printing to construct the reaction zone, and screen-printed carbon ink-based bipolar and driving electrodes onto the paper. They modified the bipolar electrode via hybridization chain reaction. After stimulation of the target cells followed by releasing $H_2O_2$, they recorded the ECL response of the luminol-$H_2O_2$ which served as a quantitative signal for the determination of cancer cells [30].

In 2022, Yu et al. constructed a paper-based BP-ECL analytical platform for sensitive M.SssI methyltransferase detection. The paper patterns were ingeniously designed and printed on cellulose paper. They employed pencil graphite with excellent electrical

conductivity as the bipolar electrodes to simplify the manufacturing process and reduce the costs. Taking advantage of HpaII endonuclease's ability to identify particular sequences, their C-BP-ECL system demonstrated remarkable stability, satisfactory reproducibility, and an extensive range for detecting M.SssI Methyltransferase [27].

BP-ECL techniques have also shown promising potential in the detection and quantification of ions and various small molecules [7, 31-34].

For example, Zhang and his colleagues introduced a microfluidic-based BP-ECL system with two-direction driving electrodes and a dual-channel configuration for the first time. They applied the $Ru(bpy)_3^{2+}$/tri propylamine ECL system to create the dual-channel BP-ECL sensing platform. To showcase the potential applications of this device, the detection of dopamine, $H_2O_2$, $K_3Fe(CN)_6$, and tripropylamine was examined as model targets. Their findings demonstrated that the utilization of the supporting channel enabled the detection of electroactive analytes that were not directly linked to the ECL reaction. [35].

In 2014, Wang research group investigated a full-featured ECL sensing platform based on a three-channel C-BP system for the first time. They detected $H_2O_2$, ascorbic acid, tripropylamine, glucose, and blood sugar in the modified indium tine oxide (ITO) cathodes by electrodeposited Pt as a bipolar electrode in a three-channel C-BP-ECL device with good performance [36].

Caffeic acid (CA) (3, 4-dihydroxy-cinnamic acid; $C_9H_8O_4$) is a phenolic compound which is produced as a peripheral metabolism of some herbage products like coffee beans, olives, carrots and fruits [37]. Also it is well-known as an antioxidant existing in wines, teas, coffee, olive oils, etc [38]. Previous studies showed multiple vital physiological effects of CA including antioxidant [39-41], antibacterial [42-44], antiviral [45-48], anti-inflammatory effects [49, 50], antidiabetic [51, 52], cardioprotective [53, 54], anticancer [55-60], etc.

Although CA plays a vital role in the human body, an excessive dose of it can lead to negative side effects [49, 50]. Therefore, the development of new methods for the quantitative analysis of CA in dietary supplements, foods and pharmaceuticals is very important [61-63]. During recent years several analytical methods have been investigated for CA quantitative measurements, which includes high performance liquid chromatography, capillary electrophoresis, spectrophotometry, and mass spectrometry as well as electrochemical methods [64-66]. Among these techniques, electrochemical methods have

been increasingly employed in the detection of CA [67, 68]. But these methods have several limitations like time consuming, highly cost effective, complex detection procedure, etc. [67, 69]. Therefore, the development of hand hold sensors with impressive features like highly sensitivity and selectivity, simple setup, possibility of miniaturization and rapidity is very important [68].

Herein, we present a multichannel bipolar sensing platform that enables the sensitive monitoring of CA using the robust ECL technique. This design allows for the detection of CA in both oxidation and reduction pathways within a single device. Scheme 1 presents an illustration of the configuration and operation mechanism of the three-channel C-BP system. The device consists of three distinct reservoirs that are connected through a set of two pairs of gold rods acting as bipolar electrodes and two gold rods functioning as driving electrodes, which are integrated into the overall system. Furthermore, to establish a more accurate mechanism for bipolar systems, the color changes of the universal pH indicator were analyzed. Finally, the effectiveness of the design was shown by successfully detecting CA in two different pathways within a single chip.

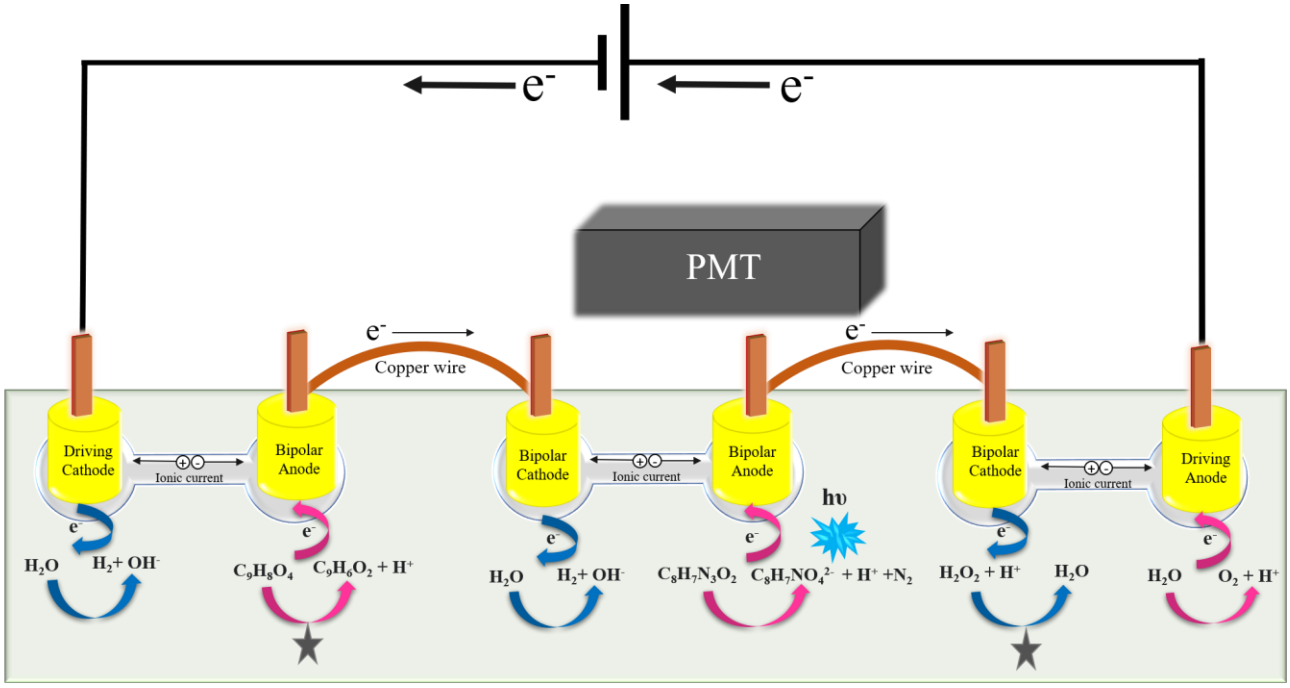


**Scheme 1**. Structure of the full-featured ECL sensing platform for monitoring of CA in its oxidation pathway (in the process of CA detection within its reduction pathway, the place of analytes marked with asterisks are replaced together).

## 2. Experimental

### *2.1. Chemicals*

All chemicals were of analytical grades and were used without further purification. CA (3,4-dihydroxy-cinnamic acid), luminol, thymol blue, methyl red, bromothymol blue, phenolphthalein, potassium sulfate, sodium phosphate, disodium phosphate, sodium hydroxide, sodium acetate, acetic acid, borax, boric acid, sulfuric acid, potassium permanganate, sodium oxalate and hydrogen peroxide 30% all were acquired from commercial sources (Merck or Sigma). CA stock solution and luminol solution were prepared daily by dissolving appropriate amount of CA and luminol in phosphate buffer (0.05 mol $L^{-1}$, pH 7.0) and borate buffer (0.05 mol $L^{-1}$, pH 9.0), respectively. Hydrogen peroxide was standardized weekly using $Na_2C_2O_4$ and $KMnO_4$. Different pH values of phosphate buffer solutions (0.05 mol $L^{-1}$) were prepared by using $NaH_2PO_4$ and $Na_2HPO_4$ salts. $CH_3COOH$ and $CH_3COONa$ were used for the preparation of a 0.05 M acetate buffer solution. Borate buffer solutions (0.05 mol $L^{-1}$) were prepared using $Na_2[B_4O_5(OH)_4]\cdot 8H_2O$ and $H_3BO_3$. The pH adjustment was achieved using NaOH and HCl solutions (0.1 mol $L^{-1}$).

### *2.2. Apparatus*

Six gold rods, each with a diameter of 4 mm, were utilized as both driving and bipolar electrodes. Two of these rods were utilized as driving electrodes and positioned within the microchannel's side terminals. Four of the gold rods were interconnected in pairs using copper wires and then employed as bipolar electrodes. A DC power supply (ERAM TRONICS, Iran) was employed to apply a constant voltage ($E_{app}$) to the gold driving electrodes. The adjustment of pH was implemented with a pH-meter (Metrohm model 691). The ECL responses were monitored using a photomultiplier (PMT) (Hamamatsu, USA) connected to an oscilloscope (MEGATEK, China) at room temperature. A Nikon AF-S Nikkor 50mm f/1.8G digital camera was employed to capture the visual ECL from the electrodes within a darkroom setting.

### *2.3. Device fabrication*

The microchannel of the C-BP-ECL was designed using AutoCAD software, and then the design was converted to the STL format. The BPE cell was constructed by Mankati Fullscale XT Plus printer. It is composed of three microchannels. These microchannels were printed

using the poly lactic acid (PLA) filament. Each of the microchannels had a 12 mm length and the diameter of each reservoir was 5 mm. The overall dimensions of the devices are 1 × 6 × 0.4 $cm^3$. Two gold rods, as the driving anode and driving cathode, were placed at an interval of 5.2 cm of each other on two-terminal sides of the sensing reservoirs (Scheme 1).

*2.4. Mechanism demonstration*

The verifying of this multichannel C-BP-ECL was evaluated using a universal pH indicator (green, pH 7.0). Briefly, 50 μL of universal pH indicator and 10 μL $K_2SO_4$ solution (0.1 mol $L^{-1}$) were added into all reservoirs. The driving voltage (9 V) was applied to activate all the reactions.

*2.4. preparation of real sample*

Coffee powder was obtained from a supermarket and then finely powdered using a mortar and pounder. An adequate amount (2 g) of the collected sample was separately transferred into a flask containing 50 ml of Milli-Q water. After heating for 1 hour, the resulting solution was centrifuged at 4000 rpm to obtain a clear supernatant. Finally, the solution was diluted with a 0.05 mol $L^{-1}$ phosphate buffer solution and subsequently subjected to ECL analysis. The same procedure was employed for the analysis of the sample using UV-Vis spectroscopy, with the exception that Milli-Q water was used to dilute the final solution.

## 3. Results and discussion

*3.1. C-BP-ECL assay procedure and data analysis*

The procedure of the C-BP-ECL assay was outlined as follows: initially, two gold rods were inserted into the reservoirs and served as driving electrodes. Additionally, two pairs of gold rods were employed as bipolar electrodes and inserted into the microchannel (according to scheme 1). Then 50 μL borate buffer solution containing luminol/$H_2O_2$ was introduced into the reporting reservoir. Subsequently, 50 μL of a phosphate buffer solution containing CA solution or $H_2O_2$ solution was introduced into the sensing reservoirs, with their placement exchanged depending on the oxidation or reduction of the analyte. The device was positioned on the PMT inside the black box of the lab-assembled ECL measurement setup and securely fastened with clips. The application of an adequate driving voltage to the driving electrodes induced the oxidation of $H_2O_2$, leading to the generation of reactive oxygen species (ROSs)

[70]. The interaction between the generated ROS and luminol produced an unstable endoperoxide, which rapidly decomposed into excited state 3-amino phthalate anions (3-APA*), leading to the emission of light. This light emission was recorded by the PMT. The output currents from the PMT are converted to voltages using operational amplifier current-to-voltage converters. These voltage signals are then transferred to the oscilloscope for further analysis [71]. In this way, the visualization of the intensity of photons released during the luminol oxidation reaction on the oscilloscope screen was enabled [72]. The oxidation of CA in the sensing reservoir and the oxidation of luminol in the presence of hydrogen peroxide in the reporting reservoir exhibit a direct and simultaneous relationship. Due to the connection between reservoirs in the BPE system, the ECL reaction was associated with the electron transfer processes occurring at the C-BPE [73]. Ultimately, the concentration of oxidized CA in the sensing reservoir can be measured by following the emitted photons using a PMT in the reporting reservoir [1, 74].

*3.2. Demonstration of principle*

The mechanism of the multichannel C-BP-ECL system was explored through the colour change induced by the water electrolysis (Fig.1). Two driving electrodes were subjected to an external voltage, leading to creating of a potential difference between them. If the overall applied voltage is sufficiently high, it generates an electric field in the channel that triggers the oxidation and reduction reactions at the poles of bipolar electrodes [17]. As expected, the electrolysis of water did not take place in the absence of a connection between reservoirs due to the lack of forming a complete circuit (Fig. 1B). Under the same conditions, with the connection of the separated reservoir by bipolar electrodes pH changes took place (Fig. 1C). Based on the observed colour changes, it was determined that the gold cathode accepted electrons from the external power supply, resulting in the reduction of $H_2O$. Simultaneously, $H_2O$ underwent oxidation at the bipolar anode in accordance with the principle of electric neutrality [75]. Then, electrons flowed from the copper wire to the bipolar cathode [76]. The current of electrons went on until it reached the positive terminal of the power supply. The results indicated a strong interdependence among all the reactions taking place in this design, which aligned well with recent findings [77].

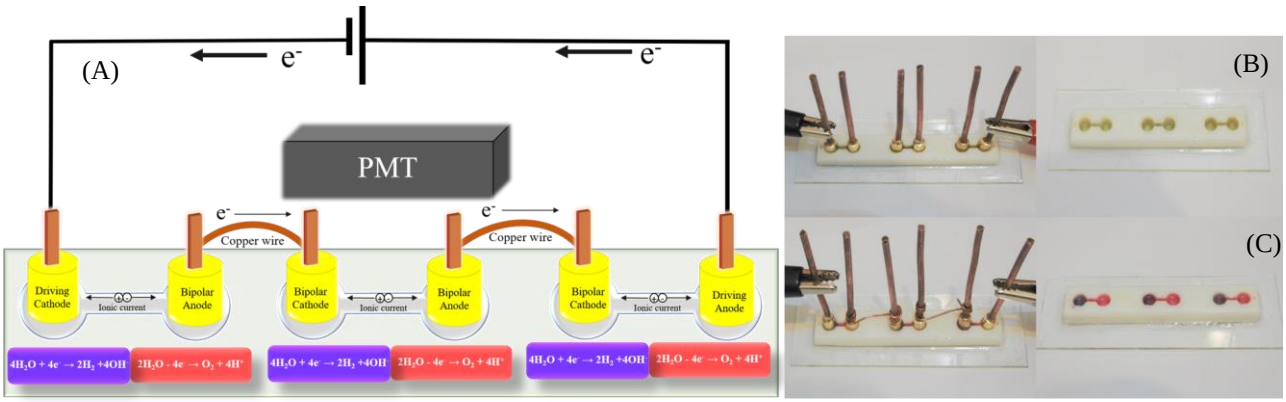


**Fig. 1**. (A) Schematic diagram of the device in mechanism study employing universal pH indicator and $K_2SO_4$ solution (B) The device without the connection between bipolar electrodes under the driving voltage of 9.0 V for 5 min, (water electrolysis did not occur and there was no change in the solution's color), (C) Device with the connection between bipolar electrodes under the driving voltage of 9.0 V for 5 min, (due to forming a complete circuit, water electrolysis occurred and a noticeable change in the solution's color was seen)

### *3.3 Optimization of effective parameters in the C-BP-ECL system*

All effective parameters on ECL intensities for the detection of CA, such as pH and concentration of luminol solution in the reporting reservoir, concentration of $H_2O_2$ as co-reactant in the reporting reservoir, pH and concentration of $H_2O_2$ in the sensing reservoir, pH of CA solution and the applied voltage to the driving electrodes, have been optimized to determine the most favorable values. In order to eliminate any background signals, the experiments were conducted both with and without the analyte in the sensing reservoir. By subtracting the ECL signal values obtained in the presence and in the absence of the analyte point by point, the net ECL signal values in the current C-BP-ECL platform were obtained. Optimal values are those where the difference in the signals (ΔECL) obtained in the presence and in the absence of the analyte is maximal.

#### *3.3.1 Optimization of pH and luminol concentration in the reporting reservoir*

ECL signals are produced by the electrochemical oxidation of luminol and the electro-generation of ROS from $H_2O_2$. Thus, the electrochemical oxidation of luminol is significantly affected by the pH and by its concentration in the solution in the reporting reservoir. ECL signal of luminol is known to be more efficient in alkaline conditions. The presence of hydroxide ions contributes to the increased efficiency of the electrochemical oxidation of luminol [78]. At high pH values, hydroxide ions help to deprotonate the luminol molecule, which increases its electron density and makes it more readily available for oxidation [79].

The optimization of pH of the luminol solution in the reporting reservoir was conducted (Fig. S1). Increasing the pH of the luminol solution up to 9.0 resulted in enhanced ECL signals for both blank and sample solutions due to the accelerated oxidation reaction of luminol [26, 80, 81]. A decrease in ECL signal at higher pH values was likely due to the decomposition of $H_2O_2$ which occurs in high alkaline media [82]. The presence of a greater concentration of hydroxide ions can act as a catalyst to speed up the decomposition of $H_2O_2$. As a consequence, the formation of oxygen gas and bubbles can lead to a reduction in the ECL signal [83].

Another influential factor on the modification of ECL intensity in C-BP-ECL platforms is the concentration of luminol. The ECL signal may be weak or difficult to detect when the luminol concentration is low. On the other hand, a high concentration of luminol may cause a reduction in the ECL signal, possibly due to quenching or interference from other sample components. The impact of luminol concentrations on ECL signals has also been explored, as shown in (Fig. S2). The increase of luminol concentration leads to an increase in the concentration of 3-amino phthalate dianion ions and subsequently intensifies ECL signals. At luminol concentrations exceeding 2.5 mmol $L^{-1}$, a decrease in the intensity of the ECL signal was observed. The self-quenching effect that occurs at high concentrations of luminol could be responsible for this phenomenon [84-86].

*3.3.2 Optimization of concentration of $H_2O_2$ as co-reactant in the reporting reservoir*

Optimizing the concentration of $H_2O_2$ in the reporting reservoir for luminol oxidation is crucial for achieving maximum ECL signal intensity and sensitivity. The electrochemical oxidation of $H_2O_2$ on the electrode surface leads to the generation of ROSs. The reaction between ROSs, particularly superoxide anion ($O_2^{\bullet-}$), and luminol results in the production of an excited state namely the 3-amino phthalate dianion ($AP^{2-*}$). Finally, the emission of light at a wavelength of 425 nm occurs as the excited state returns to the ground state [70].

According to Fig. S3, ECL signals exhibit an increase when the concentration of $H_2O_2$ is increased up to 3.0 mmol $L^{-1}$, but beyond this concentration, the signals decrease. One possible reason for the suppression of ECL could be the formation of $H^+$ during the electrochemical oxidation of $H_2O_2$, which can decrease the pH in the electrode's vicinity [87].

*3.3.3 Optimization of pH and $H_2O_2$ concentration in the sensing reservoir*

In the current C-BP-ECL design, $H_2O_2$ can undergo both oxidation and reduction reactions depending on its location within the microfluidic BPE cell. In the oxidative pathway of CA, $H_2O_2$ can undergo reduction reaction. To comply with the law of electroneutrality throughout the circuit, the electroreduction of $H_2O_2$ must occur via a direct pathway (two-electron process) [88]. The use of gold rods as bipolar electrodes in the current platform made this easy to achieve. The direct electroreduction of $H_2O_2$ on Au electrodes has been extensively studied [88-97]. The catalytic activity of Au electrodes for the reduction of $H_2O_2$ can be attributed to their unique electronic properties, surface structure, and surface chemistry. The partial filling of d-band in the high-density surface atoms of Au provides a strong binding site for $H_2O_2$ molecules [98]. This binding can lead to the formation of a $H_2O_2$-Au complex, which facilitates the direct electroreduction of $H_2O_2$ by lowering the activation energy required for the reaction [99, 100].

Due to the pH-dependent nature of the electroreduction rate of $H_2O_2$, it is imperative to achieve an optimal pH. The influence of pH of the $H_2O_2$ solution in the sensing reservoir on the ECL signal (in reporting reservoir) is shown in Fig. S4. An upward trend in ECL signal was seen in acidic medium as the pH of the $H_2O_2$ solution in the sensing reservoir is increased to 5.0. The higher equilibrium potential for the electroreduction of $H_2O_2$ in an acidic medium could be responsible for that [88]. The decrease in ECL signal at pH values greater than 5.0 (specifically in alkaline conditions) could be associated with the self-decomposition of $H_2O_2$ [101].

To minimize the chemical decomposition of $H_2O_2$, the concentration of $H_2O_2$ in the sensing reservoir was optimized. Fig. S5 shows that the maximum ECL signal was achieved at a concentration of 7.0 mmol $L^{-1}$. This concentration was chosen because, within the experimental timeframe, no oxygen bubbles were observed on the electrode, suggesting that the degradation of $H_2O_2$ could be neglected [88].

*3.3.4 Optimization of the pH of the CA solution in the sensing reservoir*

The redox behavior of CA typically entails the transfer of two electrons and two protons; hence it is affected by the pH of the medium [102-105]. Thus, the effect of pH of the CA solution was explored on ECL signal. As displayed in Fig. S6, CA oxidation at pH 7.0. results in maximum ECL signal in the reporting reservoir. One possible reason is that the

redox reaction of CA is fully reversible at neutral pH which implies a fast reaction kinetics of CA redox in this condition [64, 66, 106].

*3.3.5 Optimization of applied voltage*

The applied voltage to the driving electrodes significantly affects the rate of electrochemical oxidation of luminol to 3-amino phthalate, and consequently, the ECL signals. As depicted in Fig. 2, an increase in the applied voltage up to 9.0 V led to enhanced ΔECL intensities. However, applying voltages exceeding 9.0 V was found to reduce the ECL signals. This can be attributed to the formation of bubbles on the bipolar electrode surface resulting from water oxidation, which causes both chemical and physical interference with ECL emission [75, 107]. The results indicate that an $E_{app}$ of 9.0 V is the optimal value for achieving a strong target signal with a high signal-to-noise ratio.

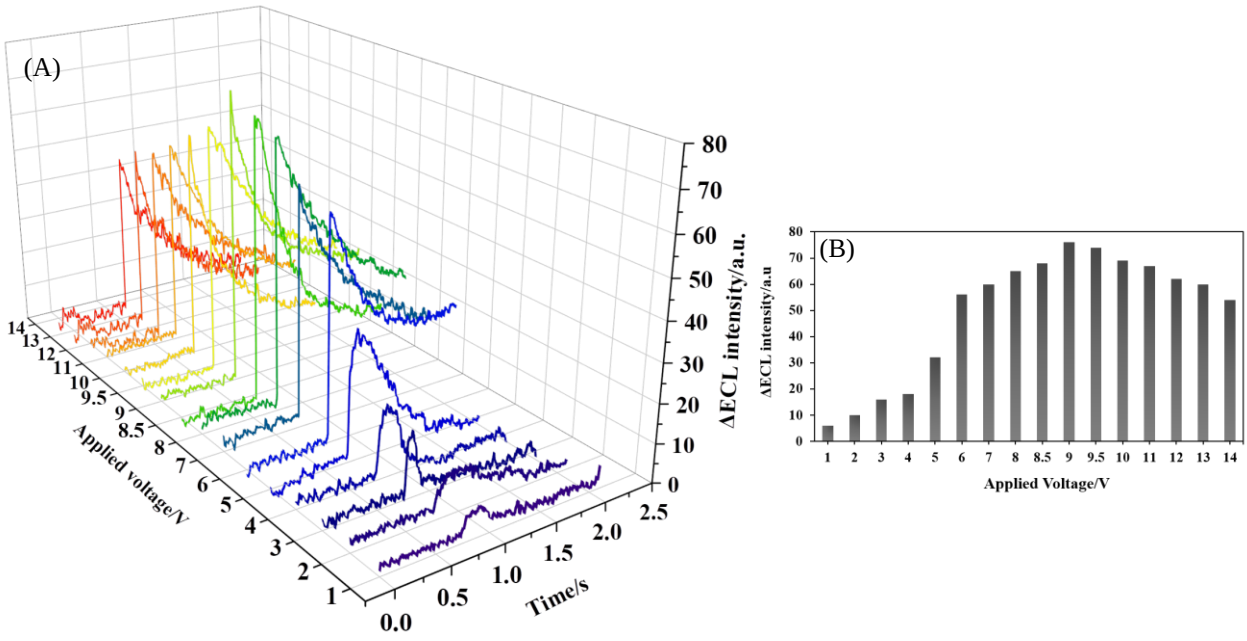


**Fig. 2.** A) ΔECL response and B) ΔECL intensity to the different driving voltage (pH of CA in sensing reservoir: 7.0, pH of luminol: 9.0, concentration of luminol in reporting reservoir: 2.5 mM, concentration of $H_2O_2$ in sensing reservoir: 7.0 mM, concentration of $H_2O_2$ as co-reactant in reporting reservoir: 3.0 mM, pH of $H_2O_2$ in sensing reservoir: 5.0, concentration of CA in sensing reservoir: 0.7 mM).

*3.4 Analytical performance of the C-BPE-ECL system for the quantitative measurement of CA*

*3.4.1 PMT-based CA detection*

Under optimized conditions, CA was detected in our design by monitoring the signal of the ECL reaction taking place at the bipolar anode, for the first time. In order to specify the signal associated with the analyte concentration, the ECL values were subtracted from that of a blank control sample. Fig. 3A demonstrates a gradual increase in the ΔECL intensity as the concentration of CA in the sensing reservoir increases. A wide linear range from 5 μmol $L^{-1}$ to 700 μmol $L^{-1}$ with $R^2$ of 0.9953 was found (Fig. 6B), and the corresponding limit of detection (LOD) was calculated to be 1.2 μmol $L^{-1}$ (S/N = 3).

To demonstrate the potential application of the present full-featured closed bipolar sensing platform, the detection of CA was also performed in the direction of reduction of it.

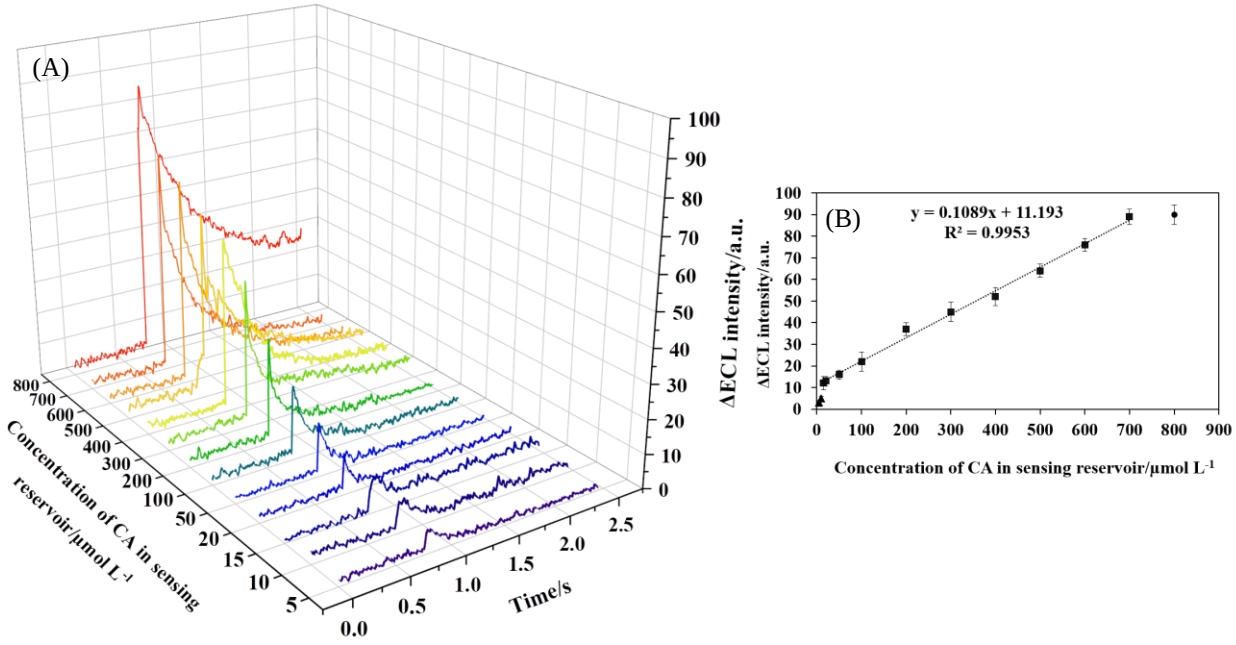


**Fig. 3.** A) ΔECL response of the different concentration of CA (oxidative pathway), B) related calibration curve (driving voltage: 9.0 V, pH of CA in sensing reservoir: 7.0, pH of luminol: 9.0, concentration of luminol in reporting reservoir: 2.5 mM, concentration of $H_2O_2$ in sensing reservoir: 7.0 mM, concentration of $H_2O_2$ as coreactant in reporting reservoir: 3.0 mM, pH of $H_2O_2$ in sensing reservoir: 5.0).

For this purpose, the positions of CA and $H_2O_2$ were swapped on opposite sides of the sensing reservoir. In this particular configuration, $H_2O_2$ underwent oxidation on the bipolar

anode, while CA was reduced on the bipolar cathode. As shown in Fig. 3B, the linear relationship between ΔECL intensity and CA concentration was from 30 μmol $L^{-1}$ to 450 μmol $L^{-1}$ ($R^2$ = 0.9911), and the detection limit was 8.6 μmol $L^{-1}$.

The obtained results demonstrate that the proposed multichannel closed bipolar sensing platform is highly suitable for detecting a wide range of targets, regardless of whether they undergo oxidation or reduction. This platform exhibits exceptional sensitivity, selectivity, and throughput capabilities, making it a promising solution for various analytical applications.

Table S1 presents a comparison between the current method and recent reports on CA detection. While the LOD and linear range of our sensor may not be as optimal as those reported for other electrochemical sensors used in CA detection, we are confident that the performance of the proposed assay can be greatly improved by modifying the sensing electrode with materials including graphene/carbon nanotubes, metallic nanomaterials, or even biomolecules that can generate a robust current during CA oxidation. Further investigation is still underway in this particular research direction.

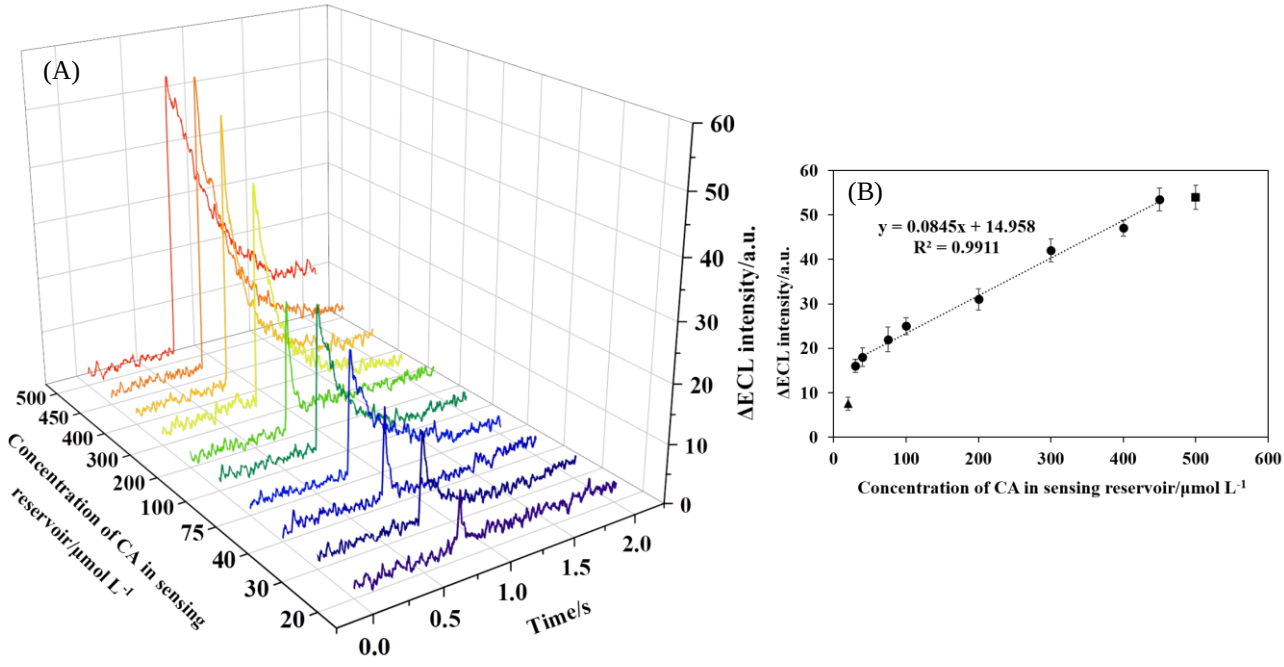


**Fig. 4.** A) ΔECL response of the different concentration of CA (reductive pathway), B) related calibration curve

*3.4.2 Visual-based CA detection*

Utilizing a PMT is a common approach for capturing the signal generated by ECL intensities. However, the need for portable, affordable, user-friendly solutions that can collect data without relying on sophisticated equipment or optical alignment has led to the emergence of digital cameras as viable ECL detectors for point-of-care testing. The visual detection technique relies on initially analyzing RGB intensity algorithms and subsequently converting the RGB image into a grayscale representation. The process of converting an RGB image into a grayscale image entails converting the color information of each pixel in the image into a single intensity value [108]. These alternative light sensors have gained significant popularity due to their acceptable sensitivity and ability to fulfill the urgent demand for practical and cost-effective solutions [19].

To visually determine CA, the ECL signal of the bipolar anode in reporting reservoir was captured using a digital camera within a dark room environment. As anticipated, there was a gradual increase in the ECL intensity as the concentration of oxidized CA increased (Fig. 5A). Fig. 5B illustrates a linear correlation between the gray value of the ECL image and the concentration of oxidized CA in the range from 50 μmol $L^{-1}$ to 600 μmol $L^{-1}$ with a detection limit of 14.8 μmol $L^{-1}$ In addition, visual detection of CA was carried out in the reduction pathway of analyte as well. The ECL signals progressively increased with increasing reduced CA concentration in the range from 55 μmol $L^{-1}$ to 400 μmol $L^{-1}$ (Fig. 5A and B) and the LOD was acquired 21.2 μmol $L^{-1}$.

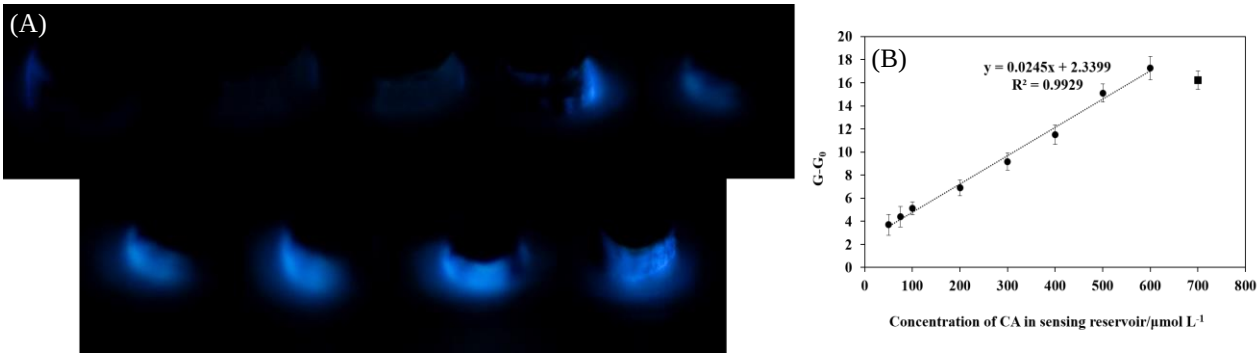

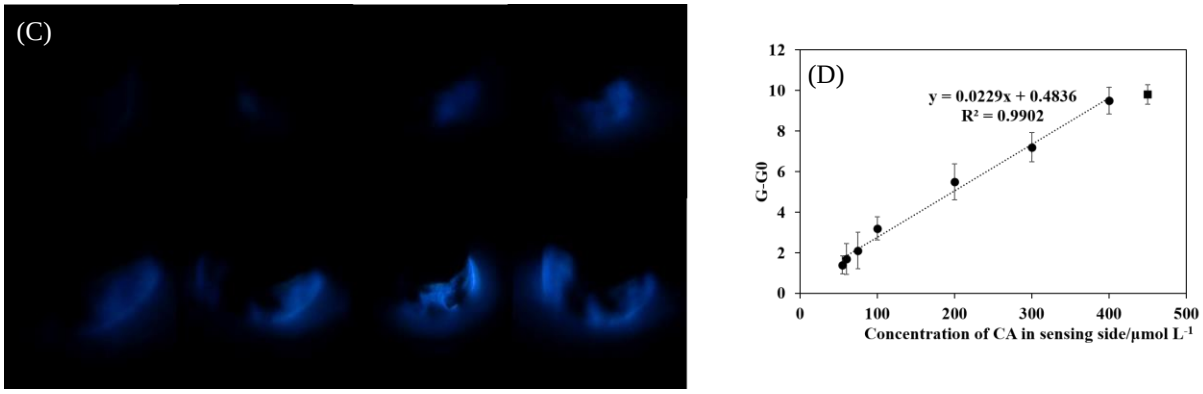


**Fig. 5.** A) ECL image of the different concentrations of the CA in optimized conditions (oxidative pathway), B) related calibration curve between the ECL image gray value and the concentration of the CA, C) ECL image of the different concentrations of the (reductive pathway), D) related calibration curve between the ECL image gray value and the concentration of the CA (Nikon camera: Lenz: 50 mm, Iso: 200, Shutter Speed: 8 s, Diaphragm: F1.8).

*3.5 Selectivity of the proposed C-BP-ECL platform*

The assessment of selectivity holds substantial importance in a newly developed ECL sensor. To evaluate the selectivity of the ECL sensor, ECL measurements were conducted in the presence of a variety of potential interfering species. A coexisting species was deemed non-interfering if the resulting relative error did not exceed 5% when measuring 400 µmol $L^{-1}$ of CA. Based on the findings summarized in Fig. S6, it was observed that 500 fold concentrations of $Na^+$, $K^+$, $I^-$, $F^-$, $NH_4^+$, $NO_3^-$, $Cl^-$, $SCN^-$, lactose, fructose, and sucrose, 200 fold concentrations of of $Sr^{2+}$, $Mg^{2+}$, $Cr^{2+}$, $Ca^{2+}$, $Al^3$, and $Mn^{2+}$, 50 fold concentrations of L-cysteine, tyrosine, glucose, and 3 fold concentrations of concentrations of catechol, gallic acid, ascorbic acid, hydroquinone, and uric acid, did not significantly interfere with the monitoring of CA. Therefore, a substantial number of structurally similar compounds effectively interfered with a constant CA concentration. The addition of interfering compounds led to a minor fluctuation in the ECL response of CA, with the variation not exceeding 5%.

*3.6 Application of the C-BP-ECL platform for real sample analysis*

The potential applicability of the proposed method was evaluated for the measurement of CA in coffee sample. To validate the findings, the results obtained from the proposed C-BP-ECL sensing platform were compared with the results from UV-Vis spectroscopy. For this purpose, the standard addition method was employed. Fig. 6(A-F) display ΔECL responses, ECL image and UV-Vis spectra for the consecutive addition of CA standard

solution to the unknown samples and the corresponding standard addition curves. It can be observed that there is a linear correlation between the responses and the added concentration of the standards. Table S2 displays the results of CA determinations obtained through UV-Vis spectroscopy and the suggested ECL sensing platform. The recoveries and relative standard deviations (RSDs) obtained indicate the excellent accuracy and precision of the proposed assay for actual detection. The t-values for each determination fall within the range of 0.142 to 2.52 and are lower than 4.13 (the critical t-value at a 95% confidence level for 2 degrees of freedom), indicating that there is no significant discrepancy between the measured values and the actual values. Finally, The ANOVA test result indicated that the CA concentrations determined by these three methods did not demonstrate statistically significant differences. Hence, the C-BP-ECL platform may present an alternative instrument for the measurement of CA in various research and application areas.

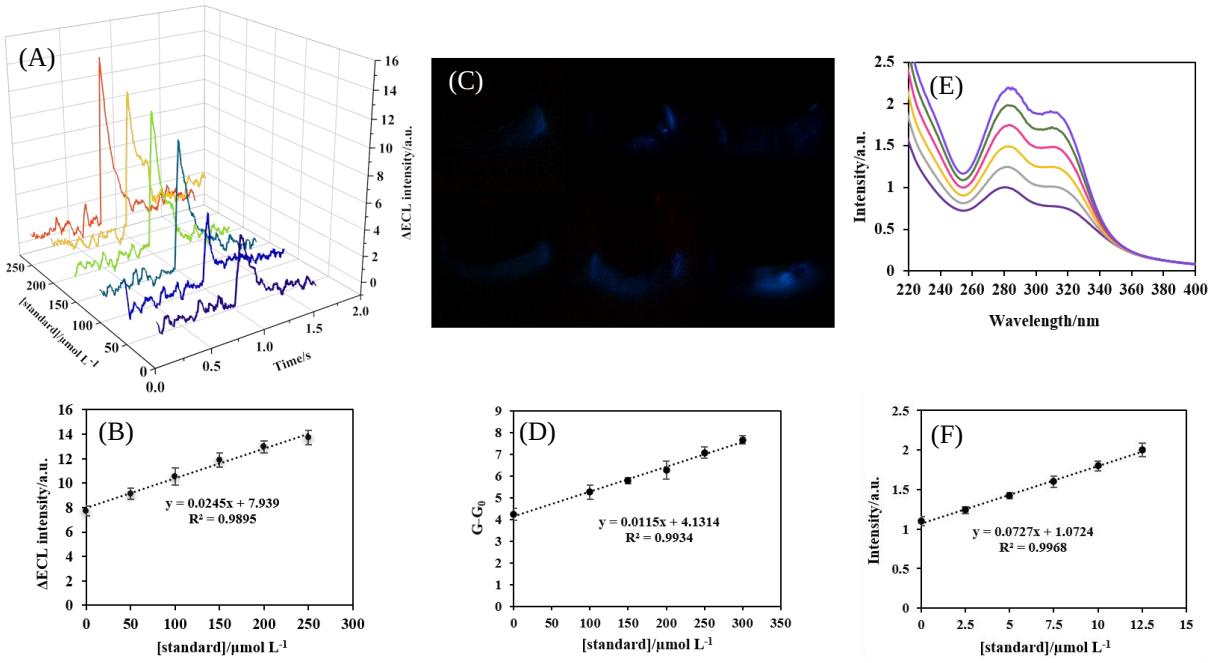


**Fig. 6.** A, C, E) ΔECL response, ECL image and UV-Vis spectrum of different concentration of added standard CA, respectively, B, D, F) corresponding calibration plot between by ΔECL response, ECL image and UV-Vis spectrum and different concentration of added standard CA, respectively.

## 4. Conclusions

We have presented a full-featured ECL sensing platform based on a three-channel closed bipolar system. The C-BPE ensured a high current efficiency by allowing the current to pass exclusively through the bipolar electrode. The multichannel and BPE configuration enabled

the successful analysis of CA with good performance in both its oxidation and reduction pathway. The results revealed the promising potential of our device for real-time analysis of CA that was directly related to the ECL process. By employing this strategy, we have developed a sensing method that can directly convert a chemical reaction into a visible readout signal, eliminating the need for complex instrumentation. In summary, the microfluidic bipolar sensing platform presented in this study, featuring a novel bipolar system design, shows significant potential for the development of highly integrated, automated, and high-throughput electrochemical or ECL devices. The designed device holds promising prospects for applications in medicinal and food monitoring. Ongoing research is being conducted to further explore its capabilities and potential.

**Acknowledgement**

The authors thank the research Council of University of Alzahra University for financial support of this work.

**Declaration of Interest Statement**

The authors declare that they have no known competing financial interests or personal relationships that could have appeared to influence the work reported in this paper.

**Supplementary materials**

Supplementary material associated with this article can be found in the online version.

## Reference

[1] L. Bouffier, S. Arbault, A. Kuhn, N. Sojic, Generation of electrochemiluminescence at bipolar electrodes: concepts and applications, Analytical and bioanalytical chemistry, 408 (2016) 7003-7011.
[2] M. Shokouhi, M.A. Mehrgardi, Cancer Cell Detection-Based on Released Hydrogen Peroxide Using a Non-Modified Closed Bipolar Electrochemical System, ChemElectroChem, 7 (2020) 3439-3444.
[3] S.E. Fosdick, K.N. Knust, K. Scida, R.M. Crooks, Bipolar electrochemistry, Angewandte Chemie International Edition, 52 (2013) 10438-10456.

[4] R. Poorghasem, R.S. Saberi, M. Shayan, M.A. Mehrgardi, A. Kiani, Closed bipolar electrochemistry for the detection of human immunodeficiency virus short oligonucleotide, Electrochimica Acta, 222 (2016) 1483-1490.
[5] A. Ismail, S. Voci, P. Pham, L. Leroy, A. Maziz, L. Descamps, A. Kuhn, P. Mailley, T. Livache, A. Buhot, Enhanced bipolar electrochemistry at solid-state micropores: Demonstration by wireless electrochemiluminescence imaging, Analytical chemistry, 91 (2019) 8900-8907.
[6] M. Wu, N. Xu, J. Qiao, J. Chen, L. Jin, Bipolar electrode-electrochemiluminescence (ECL) biosensor based on a hybridization chain reaction, Analyst, 144 (2019) 4633-4638.
[7] M.R. Moghaddam, S. Carrara, C.F. Hogan, Multi-colour bipolar electrochemiluminescence for heavy metal ion detection, Chemical Communications, 55 (2019) 1024-1027.
[8] S. Yu, M. Mehrgardi, C. Shannon, A bipolar electrochemical sensor with square wave excitation and ECL readout, Electrochemistry Communications, 88 (2018) 24-28.
[9] N. Zhang, H. Gao, C.-H. Xu, Y. Cheng, H.-Y. Chen, J.-J. Xu, An efficient electrochemiluminescence enhancement strategy on bipolar electrode for bioanalysis, Analytical chemistry, 91 (2019) 12553-12559.
[10] Z. Tian, L. Mi, Y. Wu, F. Shao, M. Zou, Z. Zhou, S. Liu, Visual electrofluorochromic detection of cancer cell surface glycoprotein on a closed bipolar electrode chip, Analytical chemistry, 91 (2019) 7902-7910.
[11] X. Zhang, R.A. Lazenby, Y. Wu, R.J. White, Electrochromic, closed-bipolar electrodes employing aptamer-based recognition for direct colorimetric sensing visualization, Analytical chemistry, 91 (2019) 11467-11473.
[12] X. Zhang, C. Chen, J. Yin, Y. Han, J. Li, E. Wang, Portable and visual electrochemical sensor based on the bipolar light emitting diode electrode, Analytical chemistry, 87 (2015) 4612-4616.
[13] K.-F. Chow, B.-Y. Chang, B.A. Zaccheo, F. Mavré, R.M. Crooks, A sensing platform based on electrodissolution of a Ag bipolar electrode, Journal of the American Chemical Society, 132 (2010) 9228-9229.
[14] Y. Zhao, J. Descamps, Y. Léger, L. Santinacci, S. Zanna, N. Sojic, G. Loget, Upconversion photoinduced electrochemiluminescence of luminol-H2O2 at Si/SiOx/Ni photoanodes, Electrochimica Acta, 444 (2023) 142013.
[15] X. Fu, J. Huang, X. Lai, J. Rong, G. Qi, Z. Lin, F. Fu, Y. Dong, Strategy and mechanism for strong and stable electrochemiluminescence of graphitic carbon nitride, Electrochimica Acta, 444 (2023) 142025.
[16] Z. Dong, F. Du, T.H. Barkae, K. Ji, F. Liu, D. Snizhko, Y. Guan, G. Xu, Luminol electrochemiluminescence by combining cathodic reduction and anodic oxidation at regenerable cobalt phthalocyanine modified carbon paste electrode for dopamine detection, Electrochimica Acta, 441 (2023) 141774.
[17] M. Bhaiyya, P.K. Pattnaik, S. Goel, A brief review on miniaturized electrochemiluminescence devices: From fabrication to applications, Current Opinion in Electrochemistry, 30 (2021) 100800.
[18] Z.-Y. Che, X.-Y. Wang, X. Ma, S.-N. Ding, Bipolar electrochemiluminescence sensors: From signal amplification strategies to sensing formats, Coordination Chemistry Reviews, 446 (2021) 214116.
[19] S.M. Khoshfetrat, H. Khoshsafar, A. Afkhami, M.A. Mehrgardi, H. Bagheri, Enhanced visual wireless electrochemiluminescence immunosensing of prostate-specific antigen based on the luminol loaded into MIL-53 (Fe)-NH2 accelerator and hydrogen evolution reaction mediation, Analytical chemistry, 91 (2019) 6383-6390.
[20] C. Chen, Y.-L. Wang, X. Lin, S.-H. Ma, J.-T. Cao, Y.-M. Liu, Cu-MOFs/GOx Bifunctional Probe-Based Synergistic Signal Amplification Strategy: Toward Highly Sensitive Closed Bipolar Electrochemiluminescence Immunoassay, ACS Applied Materials & Interfaces, 15 (2023) 22959-22966.
[21] Y.-L. Jia, X.-Q. Li, H.-Y. Chen, W. Zhao, J.-J. Xu, Simultaneous Detection of Alzheimer's Biomarkers using a Visual Electrochemiluminescence Bipolar Array, Sensors and Actuators B: Chemical, (2023) 134591.
[22] X. Li, X. Qin, Z. Tian, K. Wang, X. Xia, Y. Wu, S. Liu, Gold nanowires array-based closed bipolar nanoelectrode system for electrochemiluminescence detection of α-fetoprotein on cell surface, Analytical Chemistry, 94 (2022) 7350-7357.

[23] Y. Su, W. Lai, Y. Liang, C. Zhang, Novel cloth-based closed bipolar solid-state electrochemiluminescence (CBP-SS-ECL) aptasensor for detecting carcinoembryonic antigen, Analytica Chimica Acta, 1206 (2022) 339789.
[24] F. Wang, C. Fu, C. Huang, N. Li, Y. Wang, S. Ge, J. Yu, based closed Au-Bipolar electrode electrochemiluminescence sensing platform for the detection of miRNA-155, Biosensors and Bioelectronics, 150 (2020) 111917.
[25] J. Zhao, C.-X. Chen, J.-W. Zhu, H.-L. Zong, Y.-H. Hu, Y.-Z. Wang, Ultrasensitive and visual electrochemiluminescence ratiometry based on a constant resistor-integrated bipolar electrode for MicroRNA detection, Analytical Chemistry, 94 (2022) 4303-4310.
[26] H. Motaghi, S. Ziyaee, M.A. Mehrgardi, A.A. Kajani, A.-K. Bordbar, Electrochemiluminescence detection of human breast cancer cells using aptamer modified bipolar electrode mounted into 3D printed microchannel, Biosensors and Bioelectronics, 118 (2018) 217-223.
[27] L. Zhu, X. Lv, H. Yu, X. Tan, Y. Rong, W. Feng, L. Zhang, J. Yu, Y. Zhang, based bipolar electrode electrochemiluminescence platform combined with pencil-drawing trace for the detection of M. SssI methyltransferase, Analytical Chemistry, 94 (2022) 8327-8334.
[28] W. Lai, Y. Shi, J. Zhong, X. Zhou, Y. Yang, Z. Chen, C. Zhang, A dry chemistry-based electrochemiluminescence device for point-of-care testing of alanine transaminase, Talanta, 256 (2023) 124287.
[29] X.-Y. Yang, Y.-Y. Bai, Y.-Y. Huangfu, W.-J. Guo, Y.-J. Yang, D.-W. Pang, Z.-L. Zhang, Ultrasensitive electrochemiluminescence biosensor based on closed bipolar electrode for alkaline phosphatase detection in single liver cancer cell, Analytical Chemistry, 93 (2020) 1757-1763.
[30] S. Ge, J. Zhao, S. Wang, F. Lan, M. Yan, J. Yu, Ultrasensitive electrochemiluminescence assay of tumor cells and evaluation of H2O2 on a paper-based closed-bipolar electrode by in-situ hybridization chain reaction amplification, Biosensors and Bioelectronics, 102 (2018) 411-417.
[31] W. Zhao, Y. Ma, J. Ye, J. Jin, A closed bipolar electrochemiluminescence sensing platform based on quantum dots: A practical solution for biochemical analysis and detection, Sensors and Actuators B: Chemical, 311 (2020) 127930.
[32] S.M. Khoshfetrat, H. Bagheri, M.A. Mehrgardi, Visual electrochemiluminescence biosensing of aflatoxin M1 based on luminol-functionalized, silver nanoparticle-decorated graphene oxide, Biosensors and Bioelectronics, 100 (2018) 382-388.
[33] H. Yu, H. Yang, W. Liu, L. Jin, B. Jin, M. Wu, Novel electrochemiluminescence biosensor of fumonisin B1 detection using MWCNTs-PDMS flexible bipolar electrode, Talanta, 257 (2023) 124379.
[34] L. Jin, H. Yu, W. Liu, Z. Xiao, H. Yang, B. Jin, M. Wu, Visual Measurement of Fumonisin B1 with Bipolar Electrodes Array-Based Electrochemiluminescence Biosensor, Chemosensors, 11 (2023) 451.
[35] X. Zhang, C. Chen, J. Li, L. Zhang, E. Wang, New insight into a microfluidic-based bipolar system for an electrochemiluminescence sensing platform, Analytical chemistry, 85 (2013) 5335-5339.
[36] X. Zhang, J. Li, X. Jia, D. Li, E. Wang, Full-featured electrochemiluminescence sensing platform based on the multichannel closed bipolar system, Analytical chemistry, 86 (2014) 5595-5599.
[37] D. Yang, Z. Huang, W. Jin, P. Xia, Q. Jia, Z. Yang, Z. Hou, H. Zhang, W. Ji, R. Han, DNA methylation: a new regulator of phenolic acids biosynthesis in Salvia miltiorrhiza, Industrial Crops and Products, 124 (2018) 402-411.
[38] J. Kim, S.Y. Soh, H. Bae, S.-Y. Nam, Antioxidant and phenolic contents in potatoes (Solanum tuberosum L.) and micropropagated potatoes, Applied Biological Chemistry, 62 (2019) 1-9.
[39] M. Kfoury, C. Geagea, S. Ruellan, H. Greige-Gerges, S. Fourmentin, Effect of cyclodextrin and cosolvent on the solubility and antioxidant activity of caffeic acid, Food Chemistry, 278 (2019) 163-169.
[40] C.M. Spagnol, R.P. Assis, I.L. Brunetti, V.L.B. Isaac, H.R.N. Salgado, M.A. Corrêa, In vitro methods to determine the antioxidant activity of caffeic acid, Spectrochimica Acta Part A: Molecular and Biomolecular Spectroscopy, 219 (2019) 358-366.
[41] K. Thongchai, P. Chuysinuan, T. Thanyacharoen, S. Techasakul, S. Ummartyotin, Characterization, release, and antioxidant activity of caffeic acid-loaded collagen and chitosan hydrogel composites, Journal of Materials Research and Technology, 9 (2020) 6512-6520.

[42] M. Matejczyk, R. Świsłocka, A. Golonko, W. Lewandowski, E. Hawrylik, Cytotoxic, genotoxic and antimicrobial activity of caffeic and rosmarinic acids and their lithium, sodium and potassium salts as potential anticancer compounds, Advances in medical sciences, 63 (2018) 14-21.
[43] T. Mitani, K. Ota, N. Inaba, K. Kishida, H.A. Koyama, Antimicrobial activity of the phenolic compounds of Prunus mume against Enterobacteria, Biological and Pharmaceutical Bulletin, 41 (2018) 208-212.
[44] J.-H. Kim, D. Yu, S.-H. Eom, S.-H. Kim, J. Oh, W.-K. Jung, Y.-M. Kim, Synergistic antibacterial effects of chitosan-caffeic acid conjugate against antibiotic-resistant acne-related bacteria, Marine drugs, 15 (2017) 167.
[45] Z.-M. Wu, Z.-J. Yu, Z.-Q. Cui, L.-Y. Peng, H.-R. Li, C.-L. Zhang, H.-Q. Shen, P.-F. Yi, B.-D. Fu, In vitro antiviral efficacy of caffeic acid against canine distemper virus, Microbial pathogenesis, 110 (2017) 240-244.
[46] J. Langland, B. Jacobs, C.E. Wagner, G. Ruiz, T.M. Cahill, Antiviral activity of metal chelates of caffeic acid and similar compounds towards herpes simplex, VSV-Ebola pseudotyped and vaccinia viruses, Antiviral research, 160 (2018) 143-150.
[47] Y. Ma, W. Cong, H. Huang, L. Sun, A.H. Mai, K. Boonen, W. Maryam, W. De Borggraeve, G. Luo, Q. Liu, Identification of fukinolic acid from Cimicifuga heracleifolia and its derivatives as novel antiviral compounds against enterovirus A71 infection, International journal of antimicrobial agents, 53 (2019) 128-136.
[48] J. Shen, G. Wang, J. Zuo, Caffeic acid inhibits HCV replication via induction of IFNα antiviral response through p62-mediated Keap1/Nrf2 signaling pathway, Antiviral Research, 154 (2018) 166-173.
[49] H.G. Choi, P.T. Tran, J.-H. Lee, B.S. Min, J.A. Kim, Anti-inflammatory activity of caffeic acid derivatives isolated from the roots of Salvia miltiorrhiza Bunge, Archives of pharmacal research, 41 (2018) 64-70.
[50] M. Kępa, M. Miklasińska-Majdanik, R.D. Wojtyczka, D. Idzik, K. Korzeniowski, J. Smoleń-Dzirba, T.J. Wąsik, Antimicrobial potential of caffeic acid against Staphylococcus aureus clinical strains, BioMed research international, 2018 (2018).
[51] S.-Y. Chiou, J.-M. Sung, P.-W. Huang, S.-D. Lin, Antioxidant, antidiabetic, and antihypertensive properties of Echinacea purpurea flower extract and caffeic acid derivatives using in vitro models, Journal of medicinal food, 20 (2017) 171-179.
[52] M. Yusuf, M. Nasiruddin, N. Sultana, J. Akhtar, M.I. Khan, M. Ahmad, Regulatory Mechanism of Caffeic acid on glucose Metabolism in Diabetes, Research Journal of Pharmacy and Technology, 12 (2019) 4735-4740.
[53] O.M. Agunloye, G. Oboh, A.O. Ademiluyi, A.O. Ademosun, A.A. Akindahunsi, A.A. Oyagbemi, T.O. Omobowale, T.O. Ajibade, A.A. Adedapo, Cardio-protective and antioxidant properties of caffeic acid and chlorogenic acid: Mechanistic role of angiotensin converting enzyme, cholinesterase and arginase activities in cyclosporine induced hypertensive rats, Biomedicine & Pharmacotherapy, 109 (2019) 450-458.
[54] V.F. Salau, O.L. Erukainure, M.S. Islam, Caffeic acid protects against iron-induced cardiotoxicity by suppressing angiotensin-converting enzyme activity and modulating lipid spectrum, gluconeogenesis and nucleotide hydrolyzing enzyme activities, Biological Trace Element Research, 199 (2021) 1052-1061.
[55] K.M.M. Espíndola, R.G. Ferreira, L.E.M. Narvaez, A.C.R. Silva Rosario, A.H.M. Da Silva, A.G.B. Silva, A.P.O. Vieira, M.C. Monteiro, Chemical and pharmacological aspects of caffeic acid and its activity in hepatocarcinoma, Frontiers in oncology, (2019) 541.
[56] L.P. Pelinson, C.E. Assmann, T.V. Palma, I.B.M. da Cruz, M.M. Pillat, A. Mânica, N. Stefanello, G.C.C. Weis, A. de Oliveira Alves, C.M. de Andrade, Antiproliferative and apoptotic effects of caffeic acid on SK-Mel-28 human melanoma cancer cells, Molecular biology reports, 46 (2019) 2085-2092.
[57] M. Saleem, H.A. Ali, M.F. Akhtar, U. Saleem, A. Saleem, I. Irshad, Chemical characterisation and hepatoprotective potential of Cosmos sulphureus Cav. and Cosmos bipinnatus Cav, Natural Product Research, 33 (2019) 897-900.

[58] S. Martini, A. Conte, D. Tagliazucchi, Antiproliferative activity and cell metabolism of hydroxycinnamic acids in human colon adenocarcinoma cell lines, Journal of agricultural and food chemistry, 67 (2019) 3919-3931.
[59] H. Chen, Y. Guan, S.J. Baek, Q. Zhong, Caffeic acid phenethyl ester loaded in microemulsions: enhanced in vitro activity against colon and breast cancer cells and possible cellular mechanisms, Food Biophysics, 14 (2019) 80-89.
[60] N. Zeng, T. Hongbo, Y. Xu, M. Wu, Y. Wu, Anticancer activity of caffeic acid n-butyl ester against A431 skin carcinoma cell line occurs via induction of apoptosis and inhibition of the mTOR/PI3K/AKT signaling pathway Retraction in/10.3892/mmr. 2021.12011, Molecular medicine reports, 17 (2018) 5652-5657.
[61] J. Li, Y. Bai, Y. Bai, R. Zhu, W. Liu, J. Cao, M. An, Z. Tan, Y.-x. Chang, Pharmacokinetics of caffeic acid, ferulic acid, formononetin, cryptotanshinone, and tanshinone IIA after oral administration of Naoxintong capsule in rat by HPLC-MS/MS, Evidence-based Complementary and Alternative Medicine, 2017 (2017).
[62] M. Katsarova, S. Dimitrova, L. Lukanov, F. Sadakov, Determination of phenolic acids, flavonoids, terpenes and ecdysteroids in medicinal plant extracts and food supplements, Comptes Rendus L'académie Bulg Des Sci; ResearchGate: Berlin, Germany, (2017).
[63] A.V. Bounegru, C. Apetrei, Voltammetric sensors based on nanomaterials for detection of caffeic acid in food supplements, Chemosensors, 8 (2020) 41.
[64] J.-W. Zhang, K.-P. Wang, X. Zhang, Fabrication of SnO2 decorated graphene composite material and its application in electrochemical detection of caffeic acid in red wine, Materials Research Bulletin, 126 (2020) 110820.
[65] B. Shi, L. Yang, T. Gao, C. Ma, Q. Li, Y. Nan, S. Wang, C. Xiao, P. Jia, X. Zheng, Pharmacokinetic profile and metabolite identification of bornyl caffeate and caffeic acid in rats by high performance liquid chromatography coupled with mass spectrometry, RSC advances, 9 (2019) 4015-4027.
[66] R. Nehru, Y.-F. Hsu, S.-F. Wang, Electrochemical determination of caffeic acid in antioxidant beverages samples via a facile synthesis of carbon/iron-based active electrocatalyst, Analytica Chimica Acta, 1122 (2020) 76-88.
[67] D. Bottari, L. Pigani, C. Zanardi, F. Terzi, S.V. Paţurcă, S.D. Grigorescu, C. Matei, C. Lete, S. Lupu, Electrochemical sensing of caffeic acid using gold nanoparticles embedded in poly (3, 4-ethylenedioxythiophene) layer by sinusoidal voltage procedure, Chemosensors, 7 (2019) 65.
[68] A.V. Bounegru, C. Apetrei, Voltamperometric sensors and biosensors based on carbon nanomaterials used for detecting caffeic acid—A review, International Journal of Molecular Sciences, 21 (2020) 9275.
[69] D.A. Araujo, J.R. Camargo, L.A. Pradela-Filho, A.P. Lima, R.A. Munoz, R.M. Takeuchi, B.C. Janegitz, A.L. Santos, A lab-made screen-printed electrode as a platform to study the effect of the size and functionalization of carbon nanotubes on the voltammetric determination of caffeic acid, Microchemical Journal, 158 (2020) 105297.
[70] P. Zhou, S. Hu, W. Guo, B. Su, Deciphering electrochemiluminescence generation from luminol and hydrogen peroxide by imaging light emitting layer, Fundamental Research, 2 (2022) 682-687.
[71] D.M. Wang, M.X. Gao, P.F. Gao, H. Yang, C.Z. Huang, Carbon nanodots-catalyzed chemiluminescence of luminol: a singlet oxygen-induced mechanism, The Journal of Physical Chemistry C, 117 (2013) 19219-19225.
[72] R.E. Santini, H.L. Pardue, Design and evaluation of a stabilized, dual detector chemiluminescence spectrophotometer, Analytical Chemistry, 42 (1970) 706-712.
[73] C. Liu, D. Wang, C. Zhang, A novel paperfluidic closed bipolar electrode-electrochemiluminescence sensing platform: Potential for multiplex detection at crossing-channel closed bipolar electrodes, Sensors and Actuators B: Chemical, 270 (2018) 341-352.
[74] X. Zhang, Q. Zhai, H. Xing, J. Li, E. Wang, Bipolar electrodes with 100% current efficiency for sensors, ACS sensors, 2 (2017) 320-326.
[75] X. Zhang, S.-N. Ding, Graphite paper-based bipolar electrode electrochemiluminescence sensing platform, Biosensors and Bioelectronics, 94 (2017) 47-55.
[76] R.K. Anand, E. Sheridan, K.N. Knust, R.M. Crooks, Bipolar electrode focusing: Faradaic ion concentration polarization, Analytical chemistry, 83 (2011) 2351-2358.

[77] J.P. Guerrette, S.M. Oja, B. Zhang, Coupled electrochemical reactions at bipolar microelectrodes and nanoelectrodes, Analytical chemistry, 84 (2012) 1609-1616.
[78] L. Zhu, Y. Li, G. Zhu, A novel flow through optical fiber biosensor for glucose based on luminol electrochemiluminescence, Sensors and Actuators B: Chemical, 86 (2002) 209-214.
[79] F. Barni, S.W. Lewis, A. Berti, G.M. Miskelly, G. Lago, Forensic application of the luminol reaction as a presumptive test for latent blood detection, Talanta, 72 (2007) 896-913.
[80] L. Chen, C. Zhang, D. Xing, based bipolar electrode-electrochemiluminescence (BPE-ECL) device with battery energy supply and smartphone read-out: a handheld ECL system for biochemical analysis at the point-of-care level, Sensors and Actuators B: Chemical, 237 (2016) 308-317.
[81] A. Martínez-Olmos, J. Ballesta-Claver, A.J. Palma, M.d.C. Valencia-Mirón, L.F. Capitán-Vallvey, A portable luminometer with a disposable electrochemiluminescent biosensor for lactate determination, Sensors, 9 (2009) 7694-7710.
[82] M.S. Khan, W. Zhu, A. Ali, S.M. Ahmad, X. Li, L. Yang, Y. Wang, H. Wang, Q. Wei, Electrochemiluminescent immunosensor for prostate specific antigen based upon luminol functionalized platinum nanoparticles loaded on graphene, Analytical biochemistry, 566 (2019) 50-57.
[83] N.P. Evmiridis, N.K. Thanasoulias, A.G. Vlessidis, Chemiluminescence (CL) emission generated during oxidation of pyrogallol and its application in analytical chemistry. I. Effect of oxidant compound, Talanta, 46 (1998) 179-196.
[84] R. Yang, W. Dong, Y. Ren, Y. Xue, H. Cui, Luminol functionalized tin dioxide nanoparticles with catalytic effect for sensitive detection of glucose and uric acid, Analytica Chimica Acta, 1220 (2022) 340070.
[85] D. Calabria, E. Lazzarini, A. Pace, I. Trozzi, M. Zangheri, S. Cinti, M. Difonzo, G. Valenti, M. Guardigli, F. Paolucci, Smartphone-based 3D-printed electrochemiluminescence enzyme biosensor for reagentless glucose quantification in real matrices, Biosensors and Bioelectronics, 227 (2023) 115146.
[86] W. Lai, Y. Liang, Y. Su, C. Zhang, Shared-cathode closed bipolar electrochemiluminescence cloth-based chip for multiplex detection, Analytica Chimica Acta, 1206 (2022) 339446.
[87] R. Wilson, H. Akhavan-Tafti, R. DeSilva, A.P. Schaap, Comparison between acridan ester, luminol, and ruthenium chelate electrochemiluminescence, Electroanalysis: An International Journal Devoted to Fundamental and Practical Aspects of Electroanalysis, 13 (2001) 1083-1092.
[88] D. Cao, L. Sun, G. Wang, Y. Lv, M. Zhang, Kinetics of hydrogen peroxide electroreduction on Pd nanoparticles in acidic medium, Journal of Electroanalytical Chemistry, 621 (2008) 31-37.
[89] X. Li, A.A. Gewirth, SERS study of hydrogen peroxide electroreduction on a Pb-modified Au electrode, Journal of Raman Spectroscopy: An International Journal for Original Work in all Aspects of Raman Spectroscopy, Including Higher Order Processes, and also Brillouin and Rayleigh Scattering, 36 (2005) 715-724.
[90] X. Li, D. Heryadi, A.A. Gewirth, Electroreduction activity of hydrogen peroxide on Pt and Au electrodes, Langmuir, 21 (2005) 9251-9259.
[91] M. Yang, C. Zhang, L. Wang, L. Liu, J. Bai, L. Li, S. Guo, Facile construction of a novel binder-free graphene/polyimide foam-based Au electrode for H2O2 electroreduction, Materials Chemistry and Physics, 284 (2022) 125947.
[92] I. Kolthoff, J. Jordan, Oxygen induced electroreduction of hydrogen peroxide and reduction of oxygen at the rotated gold wire electrode, Journal of the American Chemical Society, 74 (1952) 4801-4805.
[93] B.N. Ferdousi, M.M. Islam, T. Okajima, T. Ohsaka, Electroreduction of peroxycitric acid coexisting with hydrogen peroxide in aqueous solution, Electrochimica acta, 53 (2007) 968-974.
[94] M.I. AwAD, C. HARNooDE, K. ToKuDA, T. OHSAKA, Simultaneous electroanalysis of peracetic acid and hydrogen peroxide using square-wave voltammetry, Electrochemistry, 68 (2000) 895-897.
[95] M.I. Awad, C. Harnoode, K. Tokuda, T. Ohsaka, Simultaneous electroanalysis of peroxyacetic acid and hydrogen peroxide, Analytical chemistry, 73 (2001) 1839-1843.
[96] R. Toniolo, A. Pizzariello, S. Susmel, N. Dossi, G. Bontempelli, Simultaneous detection of peracetic acid and hydrogen peroxide by amperometry at Pt and Au electrodes, Electroanalysis: An

International Journal Devoted to Fundamental and Practical Aspects of Electroanalysis, 18 (2006) 2079-2084.
[97] A.M. Gómez-Marín, A. Boronat, J.M. Feliu, Electrocatalytic oxidation and reduction of H 2 O 2 on Au single crystals, Russian Journal of Electrochemistry, 53 (2017) 1029-1041.
[98] T. Frederiksen, Bimetallic electrodes boost molecular junctions, Nature Materials, 20 (2021) 577-578.
[99] J. Zhang, M.B. Vukmirovic, Y. Xu, M. Mavrikakis, R.R. Adzic, Controlling the catalytic activity of platinum-monolayer electrocatalysts for oxygen reduction with different substrates, Angewandte Chemie, 117 (2005) 2170-2173.
[100] J. Greeley, J.K. Nørskov, M. Mavrikakis, Electronic structure and catalysis on metal surfaces, Annual review of physical chemistry, 53 (2002) 319-348.
[101] O. Špalek, J. Balej, I. Paseka, Kinetics of the decomposition of hydrogen peroxide in alkaline solutions, Journal of the Chemical Society, Faraday Transactions 1: Physical Chemistry in Condensed Phases, 78 (1982) 2349-2359.
[102] G. Di Carlo, A. Curulli, R.G. Toro, C. Bianchini, T. De Caro, G. Padeletti, D. Zane, G.M. Ingo, Green synthesis of gold–chitosan nanocomposites for caffeic acid sensing, Langmuir, 28 (2012) 5471-5479.
[103] S.K. Trabelsi, N.B. Tahar, R. Abdelhedi, Electrochemical behavior of caffeic acid, Electrochimica Acta, 49 (2004) 1647-1654.
[104] F.R.F. Leite, W.d.J.R. Santos, L.T. Kubota, Selective determination of caffeic acid in wines with electrochemical sensor based on molecularly imprinted siloxanes, Sensors and Actuators B: Chemical, 193 (2014) 238-246.
[105] C. Giacomelli, K. Ckless, D. Galato, F.S. Miranda, A. Spinelli, Electrochemistry of caffeic acid aqueous solutions with pH 2.0 to 8.5, Journal of the Brazilian Chemical Society, 13 (2002) 332-338.
[106] M. Ramalingam, T. Kokulnathan, P.-C. Tsai, M. Valan Arasu, N.A. Al-Dhabi, K. Prakasham, V.K. Ponnusamy, Ultrasonication-assisted synthesis of gold nanoparticles decorated ultrathin graphitic carbon nitride nanosheets as a highly efficient electrocatalyst for sensitive analysis of caffeic acid in food samples, Applied Nanoscience, (2021) 1-12.
[107] Y.-Z. Wang, W. Zhao, P.-P. Dai, H.-J. Lu, J.-J. Xu, J. Pan, H.-Y. Chen, Spatial-resolved electrochemiluminescence ratiometry based on bipolar electrode for bioanalysis, Biosensors and Bioelectronics, 86 (2016) 683-689.
[108] C. Saravanan, Color image to grayscale image conversion, 2010 Second International Conference on Computer Engineering and Applications, IEEE, 2010, pp. 196-199.